DOI: 10.3901/CJME.2009.06.791, available online at www.cjmenet.com; www.cjmenet.com.cn

Inertia Match of a 3-RRR Reconfigurable Planar Parallel Manipulator

SHAO Zhufeng, TANG Xiaoqiang*, CHEN Xu, and WANG Liping

Department of Precision Instruments and Mechanology, Tsinghua University, Beijing 100084, China

Received March 17, 2009; revised October 20, 2009; accepted October 25, 2009; published electronically October 30, 2009

Abstract: Inertia match of the parallel manipulator means the ratio of the inertial load of the parallel manipulator converted to each actuator shaft and the moment of inertia of the actuator is kept within a reasonable range. Currently there are many studies on parallel manipulators, but few mention inertia parameters and inertia match of parallel manipulators. This paper focuses on the inertia characteristics of the 3-RRR reconfigurable planar parallel manipulator. On the basis of the inverse dynamic formulations deduced with the principle of virtual work, the inertia matrix of the 3-RRR planar parallel manipulator in the actuator space is obtained in algebraic form. Then, by unifying the dimension and averaging diagonal elements of the inertia matrix, the equivalent inertia of the parallel manipulator, which is the inertial load of the parallel manipulator converted to each actuator shaft, is determined. By transforming the inertia problem of the 3-RRR parallel manipulator into that of the serial multi-bar manipulator, the practicality of the equivalent inertia deduced by inverse dynamics is demonstrated. According to the physical meaning of the inertia equation, the manipulator is divided in to three parts. Further analysis is carried out on the contribution of each part to the equivalent inertia and their distributions in the required workspace, revealing that the passive links cannot ignored in calculating the equivalent inertia of the parallel manipulator. Finally, the inertia match for the 3-RRR reconfigurable parallel manipulator under three configurations is accomplished, and reducers are selected. The equivalent inertia calculation and the inertial match results illustrate that the inertia math is a necessary step to the design of the parallel manipulator, and inertia parameters dramatically affect dynamic performances of parallel manipulators. Besides, the equivalent inertia and inertial match principles, proposed in the paper, can be widely applied in the dynamic analysis and servomotors selecting for the parallel manipulator.

Key words: inertia match, equivalent inertia, inverse dynamics, parallel manipulator

1 Introduction

Reconfigurable manipulators, which are characterized by modularity, integrability, customization and convertibility, can be easily reconfigured and can cost-effectively respond to unpredictable market changes. The parallel manipulator, which typically consists of a moving platform and a fixed base connected together by several identical limbs, is inherently symmetric and modular, and is prone to be reconfigurable[1]. The reconfigurable parallel kinematics manipulator, which is usually abbreviated as the reconfigurable parallel kinematics manipulator (RPKM) for short, is an important branch of reconfigurable manipulators. The parallel manipulator has advantages of high rigidity, high acceleration and high flexibility over the serial manipulator. In particular, the lower-mobility parallel manipulator has potentials of larger workspace, better operability and simpler structure than the 6-degree-of-freedom(DOF) parallel manipulator[2–3]. Reconfigurable planar parallel manipulators, that inherit advantages of both parallel manipulators and reconfigurable manipulators, have great prospects. An important purpose of RPKMs is the testing platform to take theories on parallel manipulators into practice[4].

Usually, in the design of parallel manipulator, actuator parameters such as the rated and maximum speed, torque and power are considered. However, in order to achieve excellent kinematics performance, the inertia match of the parallel manipulator, which means the match between the inertial load of the parallel manipulator converted to each actuator shaft and the moment of inertia of the actuator, should be fulfilled, too. In the field of the RPKM, the need for the inertia match is more obvious, due to the significant variations of the inertial load resulting from reconfigurations. Additionally, an actuator, which is a drive element, may include a gear reducer and a coupler besides a motor.

The equivalent inertia of the parallel manipulator, which indicates the inertial load of the parallel manipulator converted to each actuator shaft, should be determined first, based on the inertia matrix. It is obvious that the inverse dynamics, which is the process of deriving the driving force of each actuator from the kinematics of the manipulator and external force system exerted on it, is a convenient way to

* Corresponding author E-mail: tang-xq@mail.tsinghua.edu.cn
This research is supported by National Hi-tech Research and Development Program of China (863 Program, Grant No. 2006AA04Z133), and National Natural Science Foundation of China (Grant No. 50605035, 10778625)

obtain the inertia matrix of the parallel manipulator in the actuator space. Several approaches, such as the Newton-Euler formulation[5–7], the Lagrangian formulation[8–9], and the principle of virtual work[10–13], have been proposed. The principle of virtual work, which has been concluded as the most effective way to deduce the dynamic formulation of the parallel manipulator, is employed to obtain the inverse dynamics of the 3-RRR reconfigurable planar parallel manipulator in this paper.

Most works in the field of the RPKM concentrated on either the parameter design and optimization or the workspace comparison[1,14]. To the best of the authors' knowledge, little attention has been paid to the study of the inertia matrix or the inertia match. In fact, the inertia match of the RPKM can guarantee good kinematics performance of the manipulator, is the necessary step to the design of RPKM.

By taking the 3-RRR reconfigurable planar parallel manipulator described in section 2 as the research object, the algebraic expression of the inertia matrix converted to the actuator space is deduced, and the equivalent inertia is figured out in section 3. In section 4, the practicality of the equivalent inertia of the parallel manipulator is verified numerically. A further analysis is carried out on contributions of different parts in the 3-RRR reconfigurable planar parallel manipulator to the total equivalent inertia, in section 5. The inertia match of the 3-RRR RPKM is accomplished, and the match result is shown in section 6. At last, conclusions of the paper are given in section 7.

2 System Description

As shown in Fig. 1, the object under study is a 3-DOF parallel manipulator driven by three AC servo motors. It is a horizontally arranged 3-RRR RPKM, which consists of a moving platform, a base and three identical limbs[15]. Each limb is composed of a drive link and a passive link, which are connected together by a rotational joint. Two ends of each limb are connected to the base and the moving platform individually by a rotational joint.

The middle part of each link is a replaceable bar, whose ends are connected to rotation modules with screw bolts (see Fig. 2). The reconfigurable manipulator is equipped with three suites of replaceable bars of different stiffness but same length (the mass and moment of inertia are different), including a suite of light flexible bars, a suite of aluminum bars and a suite of steel bars. The structure of a limb is shown in Fig. 2. Actuator adapters of passive links are used to connect shafts of actuators. There are two kinds of rotation modules that are used in pair to compose rotational joints.

The reconfigurable manipulator is designed as a testing platform used to study the active vibration control of the 3-RRR parallel manipulator of different stiffness, using distributed arrays of surface-bonded lead zirconate titanate (PZT) patch sensors and actuators. It provides a perfect opportunity to the research of the equivalent inertia for parallel manipulators.

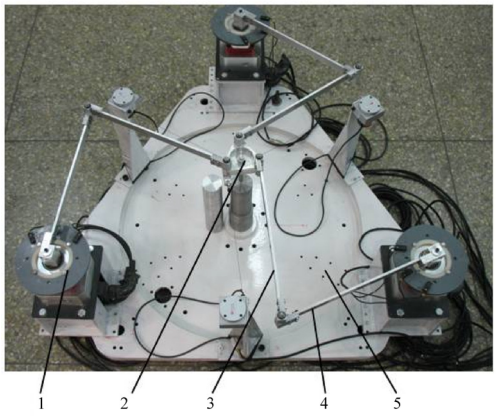

Fig. 1. 3-RRR reconfigurable planar parallel manipulator

1. Actuator; 2. Moving platform; 3. Passive link; 4. Drive link; 5. Fixed base

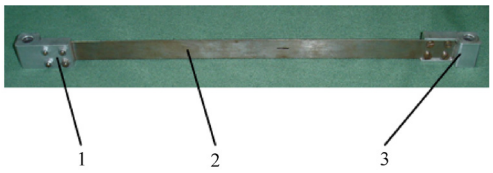

(a) Passive link

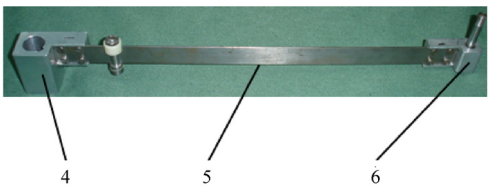

(b) Drive link

Fig. 2. Structure of a limb

1, 3, 6. Rotation module; 2, 5. Replaceable bar; 4. Actuator adapter

3 Dynamic Equations

Structure of the object can be simplified as shown in Fig. 3. Since high-speed bearings are equipped, the coulomb and viscous frictions exerted on rotational joints are reasonably neglected. The only external force exerted on the moving platform is gravity, which is eliminated from dynamic equations, due to the horizontal arrangement.

3.1 Inverse kinematics

As demonstrated in Fig. 3, a global frame $A(OXYZ)$ is attached to the geometric center of the fixed base with the X-axis parallel to A_1A_2, and the Z-axis perpendicular to the plane defined by $A_1A_2A_3$. Then, position vectors of A_i (i=1, 2, 3) in the global frame are given as

$$\boldsymbol{A}_1\left(-\frac{a}{2},-\frac{\sqrt{3}a}{6},0\right)^{\mathrm{T}},\ \boldsymbol{A}_2\left(\frac{a}{2},-\frac{\sqrt{3}a}{6},0\right)^{\mathrm{T}},\ \boldsymbol{A}_3\left(0,\frac{\sqrt{3}a}{3},0\right)^{\mathrm{T}},$$

where $|\boldsymbol{A}_1\boldsymbol{A}_2|=|\boldsymbol{A}_2\boldsymbol{A}_3|=|\boldsymbol{A}_3\boldsymbol{A}_1|=a$.

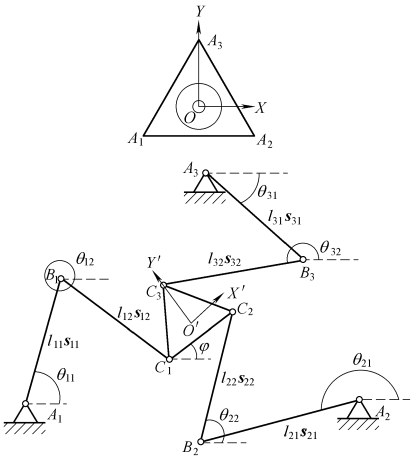

Fig. 3. Kinematic model of the 3-RRR RPKM

The moving frame $C(O'X'Y'Z')$ is located at the mass center of the moving platform with the X'-axis parallel to C_1C_2, and the Z'-axis perpendicular to the platform plane. Position vectors of $\boldsymbol{C}_i$ (i=1, 2, 3) in the moving frame are given as

$$\boldsymbol{C}_1\left(-\frac{h}{2},-\frac{\sqrt{3}h}{6},0\right)^{\mathrm{T}},\boldsymbol{C}_2\left(\frac{h}{2},-\frac{\sqrt{3}h}{6},0\right)^{\mathrm{T}},\boldsymbol{C}_3\left(0,\frac{\sqrt{3}h}{3},0\right)^{\mathrm{T}},$$

where $|\boldsymbol{C}_1\boldsymbol{C}_2|=|\boldsymbol{C}_2\boldsymbol{C}_3|=|\boldsymbol{C}_3\boldsymbol{C}_1|=h$.

Actuators are located at point $\boldsymbol{A}_i(i=1,2,3)$. The Cartesian coordinate vector of the manipulator is given by the position and orientation of the platform and can be written as

$$\boldsymbol{P}=(x,y,\varphi)^{\mathrm{T}},$$

where φ is the rotational angle of the platform about the Z-axis from the X-axis. Connection points $\boldsymbol{c}_i$ (i=1, 2, 3) (as expressed in the moving frame) can be described in the global frame by using of the platform translation $\boldsymbol{r}$ and rotation matrix $\boldsymbol{R}$ as

$$(\boldsymbol{c}_i)_{\mathrm{base}}=\boldsymbol{r}+\boldsymbol{R}\boldsymbol{c}_i.$$

Referring to Fig. 3, a vector loop equation associated with the ith limb in the global frame can be written as

$$\boldsymbol{r}+\boldsymbol{R}\boldsymbol{c}_i=\boldsymbol{r}_{A_i}+l_{i1}\boldsymbol{s}_{i1}+l_{i2}\boldsymbol{s}_{i2},\quad i=1,2,3, \tag{1}$$

where $\boldsymbol{r}=(x,y,0)^{\mathrm{T}}$ is the position vector of the moving platform; $l_{i1},l_{i2},\boldsymbol{s}_{i1}$ and $\boldsymbol{s}_{i2}$ are lengths and unit vectors of drive and passive links of the ith limb; $\boldsymbol{r}_{A_i}$ is position vector of point A_i described in the global frame, and the rotation matrix can be written as

$$\boldsymbol{R}=\begin{bmatrix}\cos\varphi & \sin\varphi & 0\\ -\sin\varphi & \cos\varphi & 0\\ 0 & 0 & 1\end{bmatrix}.$$

By setting $\boldsymbol{r}_i=\boldsymbol{r}+\boldsymbol{R}\boldsymbol{c}_i-\boldsymbol{r}_{A_i}$, we obtain

$$\boldsymbol{r}_i=l_{i1}\boldsymbol{s}_{i1}+l_{i2}\boldsymbol{s}_{i2},$$

or

$$l_{i2}\boldsymbol{s}_{i2}=\boldsymbol{r}_i-l_{i1}\boldsymbol{s}_{i1}.$$

Then, taking square of both sides of the above equation leads to

$$l_{i2}^2=\|\boldsymbol{r}_i-2l_{i1}\boldsymbol{s}_{i1}\|^2. \tag{2}$$

Substituting $\boldsymbol{s}_{i1}=(\cos\theta_i,\sin\theta_i,0)^{\mathrm{T}}$ into Eq. (2) yields three equations as follows:

$$l_{12}^2=\left[-\frac{a}{2}+l_{11}\cos\theta_{11}-\left(x-\frac{h}{2}\cos\varphi+\frac{\sqrt{3}}{6}h\sin\varphi\right)\right]^2+\left[-\frac{\sqrt{3}a}{6}+l_{11}\sin\theta_{11}-\left(y-\frac{h}{2}\sin\varphi-\frac{\sqrt{3}}{6}h\cos\varphi\right)\right]^2,$$

$$l_{22}^2=\left[\frac{a}{2}+l_{21}\cos\theta_{21}-\left(x+\frac{h}{2}\cos\varphi+\frac{\sqrt{3}}{6}h\sin\varphi\right)\right]^2+\left[-\frac{\sqrt{3}a}{6}+l_{21}\sin\theta_{21}-\left(y+\frac{h}{2}\sin\varphi+\frac{\sqrt{3}}{6}h\cos\varphi\right)\right]^2,$$

$$l_{32}^2=\left[l_{31}\cos\theta_{31}-\left(x-\frac{\sqrt{3}}{3}h\sin\varphi\right)\right]^2+\left[\frac{\sqrt{3}a}{3}+l_{31}\sin\theta_{31}-\left(y+\frac{\sqrt{3}}{3}h\cos\varphi\right)\right]^2.$$

The inverse kinematic equations for the 3-RRR RPKM is

$$\theta_{i1}=\arctan\frac{-e_{i1}\pm\sqrt{e_{i1}^2+e_{i2}^2-e_{i3}^2}}{2a},\quad i=1,2,3, \tag{3}$$

where $e_{ij}(i,j=1,2,3)$ is function that is only about x,y and φ. θ_{i1} is the rotational angle of the drive link of the ith limb. Operation symbols in above equations are determined by the assembly structure of the 3-RRR RPKM. As the model shown in Fig. 3, positive symbols should be chosen.

The unit vector along the passive link of the ith limb can be determined by

$$\boldsymbol{s}_{i2}=(\boldsymbol{r}_i-l_{i1}\boldsymbol{s}_{i1})/l_{i2},\quad i=1,2,3. \tag{4}$$

The velocity mapping function is found by taking the derivative of Eq. (1) with respect to time, i.e.

$$\dot{\boldsymbol{r}}+\boldsymbol{W}\times\boldsymbol{R}\boldsymbol{c}_i=l_{i1}\boldsymbol{W}_{i1}\times\boldsymbol{s}_{i1}+l_{i2}\boldsymbol{W}_{i2}\times\boldsymbol{s}_{i2},\quad i=1,2,3, \tag{5}$$

where $\boldsymbol{W}=(0,0,\dot{\varphi})^{\mathrm{T}}$, $\boldsymbol{W}_{i1}=(0,0,\dot{\theta}_{i1})^{\mathrm{T}}$, $\boldsymbol{W}_{i2}=(0,0,\dot{\theta}_{i2})^{\mathrm{T}}$,

$\dot{\theta}_{i1}$ and $\dot{\theta}_{i2}$ are angular velocities of drive and passive links of the *i*th limb.

Taking the dot product of Eq. (5) with $\boldsymbol{s}_{i2}$ and realizing

$$\boldsymbol{W}_{i2}\times\boldsymbol{s}_{i2}\bullet\boldsymbol{s}_{i2}=\boldsymbol{s}_{i2}\times\boldsymbol{s}_{i2}\bullet\boldsymbol{W}_{i2}=0,\quad i=1,2,3,$$

leads to

$$\boldsymbol{s}_{i2}\bullet\dot{\boldsymbol{r}}+\boldsymbol{W}\times\boldsymbol{Rc}_i\bullet\boldsymbol{s}_{i2}=l_{i1}\boldsymbol{s}_{i1}\times\boldsymbol{s}_{i2}\bullet\boldsymbol{W}_{i1},\quad i=1,2,3.$$

The angular velocity vector of the *i*th drive link is given in terms of velocities of the moving platform as

$$W_{i1}=\frac{\boldsymbol{s}_{i2}\bullet\dot{\boldsymbol{r}}+(\boldsymbol{Rc}_i\times\boldsymbol{s}_{i2})\bullet\boldsymbol{W}}{l_{i1}\boldsymbol{s}_{i1}\times\boldsymbol{s}_{i2}},\quad i=1,2,3. \tag{6}$$

Similarly, dot multiplying both sides of Eq. (5) with $\boldsymbol{s}_{i1}$ gives

$$\boldsymbol{W}_{i2}=\frac{\boldsymbol{s}_{i1}\bullet\dot{\boldsymbol{r}}+(\boldsymbol{Rc}_i\times\boldsymbol{s}_{i1})\bullet\boldsymbol{W}}{l_{i2}\boldsymbol{s}_{i2}\times\boldsymbol{s}_{i1}},\quad i=1,2,3. \tag{7}$$

Simplify Eqs. (6) and (7) as follows:

$$\dot{\theta}_{i1}=\boldsymbol{J}_{i1}\dot{\boldsymbol{P}},i=1,2,3, \tag{8}$$

$$\dot{\theta}_{i2}=\boldsymbol{J}_{i2}\dot{\boldsymbol{P}},i=1,2,3, \tag{9}$$

where

$$\boldsymbol{J}_{i1}=(\cos\theta_{i2},\sin\theta_{i2},x_{\boldsymbol{Rc}_i}\sin\theta_{i2}-y_{\boldsymbol{Rc}_i}\cos\theta_{i2})/k_{i1},$$

$$k_{i1}=l_{i1}(\cos\theta_{i1}\sin\theta_{i2}-\sin\theta_{i1}\cos\theta_{i2}),$$

$$\boldsymbol{J}_{i2}=(\cos\theta_{i1},\sin\theta_{i1},x_{\boldsymbol{Rc}_i}\sin\theta_{i1}-y_{\boldsymbol{Rc}_i}\cos\theta_{i1})/k_{i2},$$

$$k_{i2}=l_{i2}(\cos\theta_{i2}\sin\theta_{i1}-\sin\theta_{i2}\cos\theta_{i1}),$$

$$\dot{\boldsymbol{P}}=(\dot{x},\dot{y},\dot{\varphi})^{\mathrm{T}},$$

$x_{\boldsymbol{Rc}_i}$ and $y_{\boldsymbol{Rc}_i}$ are the first and second elements of $\boldsymbol{Rc}_i$.

Further, the Jacobian matrix of drive links is obtained as

$$\boldsymbol{J}_1=\begin{bmatrix}\boldsymbol{J}_{11}\\ \boldsymbol{J}_{21}\\ \boldsymbol{J}_{31}\end{bmatrix}.$$

Also, the Jacobian matrix of passive links is obtained as

$$\boldsymbol{J}_2=\begin{bmatrix}\boldsymbol{J}_{12}\\ \boldsymbol{J}_{22}\\ \boldsymbol{J}_{32}\end{bmatrix}.$$

Eqs. (8) and (9) can be rewritten in matrix form as

$$\dot{\boldsymbol{\theta}}_1=\boldsymbol{J}_1\dot{\boldsymbol{P}}, \tag{10}$$

$$\dot{\boldsymbol{\theta}}_2=\boldsymbol{J}_2\dot{\boldsymbol{P}}, \tag{11}$$

where $\dot{\boldsymbol{\theta}}_1=(\dot{\theta}_{11},\dot{\theta}_{21},\dot{\theta}_{31})^{\mathrm{T}}$, $\dot{\boldsymbol{\theta}}_2=(\dot{\theta}_{12},\dot{\theta}_{22},\dot{\theta}_{32})^{\mathrm{T}}$.

The acceleration mapping function is deduced by taking the time derivative of Eq. (5) and is expressed in terms of linear and angular acceleration vectors of the moving platform as

$$\ddot{\boldsymbol{r}}+\boldsymbol{\varepsilon}\times\boldsymbol{Rc}_i+\boldsymbol{W}\times(\boldsymbol{W}\times\boldsymbol{Rc}_i)=l_{i1}\boldsymbol{\varepsilon}_{i1}\times\boldsymbol{Rc}_i+l_{i2}\boldsymbol{\varepsilon}_{i2}\times\boldsymbol{Rc}_i+l_{i1}\boldsymbol{W}_{i1}\times(\boldsymbol{W}_{i1}\times\boldsymbol{s}_{i1})+l_{i2}\boldsymbol{W}_{i2}\times(\boldsymbol{W}_{i2}\times\boldsymbol{s}_{i2}),\quad i=1,2,3.$$

Simplifying the above function and using $\boldsymbol{s}_{ij}\bullet\boldsymbol{W}_{ij}=0$ $(i,j=1,2,3)$ leads to

$$\ddot{\boldsymbol{r}}+\boldsymbol{\varepsilon}\times\boldsymbol{Rc}_i-\boldsymbol{W}^2\boldsymbol{Rc}_i=l_{i1}\boldsymbol{\varepsilon}_{i1}\times\boldsymbol{Rc}_i+l_{i2}\boldsymbol{\varepsilon}_{i2}\times\boldsymbol{Rc}_i-l_{i1}\boldsymbol{W}_{i1}^2\boldsymbol{s}_{i1}-l_{i2}\boldsymbol{W}_{i2}^2\boldsymbol{s}_{i2},\quad i=1,2,3, \tag{12}$$

where $\boldsymbol{\varepsilon}=(0,0,\ddot{\varphi})^{\mathrm{T}}$, $\boldsymbol{\varepsilon}_{i1}=(0,0,\ddot{\theta}_{i1})^{\mathrm{T}}$, $\boldsymbol{\varepsilon}_{i2}=(0,0,\ddot{\theta}_{i2})^{\mathrm{T}}$.

By taking the dot multiply of Eq. (12) with $\boldsymbol{s}_{i2}$, the angular accelerations of drive links is obtained as

$$\boldsymbol{\varepsilon}_{i1}=\frac{\boldsymbol{s}_{i2}\bullet\ddot{\boldsymbol{r}}+(\boldsymbol{Rc}_i\times\boldsymbol{s}_{i2})\bullet\boldsymbol{\varepsilon}}{l_{i1}\boldsymbol{s}_{i1}\times\boldsymbol{s}_{i2}}+\frac{l_{i1}\boldsymbol{W}_{i1}^2\boldsymbol{s}_{i1}\bullet\boldsymbol{s}_{i2}+l_{i2}\boldsymbol{W}_{i2}^2-\boldsymbol{W}^2\boldsymbol{Rc}_i\bullet\boldsymbol{s}_{i2}}{l_{i1}\boldsymbol{s}_{i1}\times\boldsymbol{s}_{i2}},\quad i=1,2,3. \tag{13}$$

Similarly, by taking the dot product of Eq. (12) with $\boldsymbol{s}_{i1}$, the angular acceleration of passive links is obtained as

$$\boldsymbol{\varepsilon}_{i2}=\frac{\boldsymbol{s}_{i1}\bullet\ddot{\boldsymbol{r}}+(\boldsymbol{Rc}_i\times\boldsymbol{s}_{i1})\bullet\boldsymbol{\varepsilon}}{l_{i2}\boldsymbol{s}_{i2}\times\boldsymbol{s}_{i1}}+\frac{l_{i2}\boldsymbol{W}_{i2}^2\boldsymbol{s}_{i2}\bullet\boldsymbol{s}_{i1}+l_{i1}\boldsymbol{W}_{i1}^2-\boldsymbol{W}^2\boldsymbol{Rc}_i\bullet\boldsymbol{s}_{i1}}{l_{i1}\boldsymbol{s}_{i2}\times\boldsymbol{s}_{i1}},\quad i=1,2,3. \tag{14}$$

Simplify Eqs. (13) and (14) as

$$\ddot{\theta}_{i1}=\boldsymbol{J}_{i1}\ddot{\boldsymbol{P}}+f_{i1},i=1,2,3, \tag{15}$$

$$\ddot{\theta}_{i2}=\boldsymbol{J}_{i2}\ddot{\boldsymbol{P}}+f_{i2},i=1,2,3, \tag{16}$$

where

$$f_{i1}=\frac{l_{i1}\boldsymbol{s}_{i1}\bullet\boldsymbol{s}_{i2}\theta_{i1}^2+l_{i2}\theta_{i2}^2-\boldsymbol{Rc}_i\bullet\boldsymbol{s}_{i2}\varphi^2}{l_{i1}\boldsymbol{s}_{i1}\times\boldsymbol{s}_{i2}},$$

$$f_{i2}=\frac{l_{i2}\boldsymbol{s}_{i2}\bullet\boldsymbol{s}_{i1}\theta_{i2}^2+l_{i1}\theta_{i1}^2-\boldsymbol{Rc}_i\bullet\boldsymbol{s}_{i1}\varphi^2}{l_{i1}\boldsymbol{s}_{i2}\times\boldsymbol{s}_{i1}},$$

$$\dot{\boldsymbol{\theta}}_2=\boldsymbol{J}_2\dot{\boldsymbol{P}},$$

$\ddot{\theta}_{i1}$ and $\ddot{\theta}_{i2}$ are angular accelerations of drive and passive links of the *i*th limb.

Also, it is easy to derive the acceleration mapping func-

tion as

$$\ddot{\boldsymbol{\theta}}_1=\boldsymbol{J}_1\ddot{\boldsymbol{P}}+\boldsymbol{f}_1, \tag{17}$$

$$\ddot{\boldsymbol{\theta}}_2=\boldsymbol{J}_2\ddot{\boldsymbol{P}}+\boldsymbol{f}_2, \tag{18}$$

where $\ddot{\boldsymbol{\theta}}_1=(\ddot{\theta}_{11},\ddot{\theta}_{21},\ddot{\theta}_{31})^{\mathrm{T}}$, $\ddot{\boldsymbol{\theta}}_2=(\ddot{\theta}_{12},\ddot{\theta}_{22},\ddot{\theta}_{32})^{\mathrm{T}}$, $\boldsymbol{f}_1=(f_{11},f_{21},f_{31})^{\mathrm{T}}$, $\boldsymbol{f}_2=(f_{12},f_{22},f_{32})^{\mathrm{T}}$.

3.2 Inverse dynamics

In this section, the inverse dynamics of the 3-RRR RPKM is formulated by adopting the principle of virtual work. The inertia forces exerted at the mass center of the moving platform is

$$\boldsymbol{F}=(-m\ddot{x},-m\ddot{y},I\ddot{\varphi})^{\mathrm{T}},$$

where m is the mass of the moving platform which includes contributions of the payload and platform itself, I is the moment of inertia of the moving platform about its mass center.

The rotation centers A_i and C_i (i=1, 2, 3) are respectively selected as pivotal points of drive and passive links to get the most effective derivation process. The centroid of the moving platform is selected as a pivotal point too. Thus, for the 3-RRR RPKM, the virtual work principle gives

$$\sum_{i=1}^{3}\delta\boldsymbol{r}_{c_i}^{\mathrm{T}}\boldsymbol{a}_{c_i}+\delta\boldsymbol{\theta}_1^{\mathrm{T}}(\boldsymbol{\tau}-\boldsymbol{I}_1\ddot{\boldsymbol{\theta}}_1)+\delta\boldsymbol{\theta}_2^{\mathrm{T}}(-\boldsymbol{I}_2\ddot{\boldsymbol{\theta}}_2)+\delta\boldsymbol{P}^{\mathrm{T}}\boldsymbol{F}=0, \tag{19}$$

where $\delta\boldsymbol{r}_{c_i}=\boldsymbol{U}_i\delta\boldsymbol{p}$, $\boldsymbol{a}_{c_i}=-m_{i2}\boldsymbol{U}_i\ddot{\boldsymbol{p}}+m_{i2}\dot{\varphi}^2\boldsymbol{R}\boldsymbol{c}_i$,

$$\boldsymbol{U}_i=\begin{bmatrix}1 & 0 & -y_{\boldsymbol{R}\boldsymbol{c}_i}\\ 0 & 1 & x_{\boldsymbol{R}\boldsymbol{c}_i}\\ 0 & 0 & 0\end{bmatrix},\quad \boldsymbol{I}_1=\begin{bmatrix}I_{11} & & \\ & I_{21} & \\ & & I_{31}\end{bmatrix},$$

$$\boldsymbol{I}_2=\begin{bmatrix}I_{12} & & \\ & I_{22} & \\ & & I_{32}\end{bmatrix},$$

I_{i1} is the moment of inertia of the ith drive link about its pivotal point A_i, and I_{i2} is the moment of inertia of the ith passive link about its pivotal point C_i.

3.3 Inertia matrix in actuator space

Simplifying Eq. (19) leads to the inverse dynamics equation of the 3-RRR RPKM. The required input torques of the driving joints can be obtained as

$$\boldsymbol{\tau}=\boldsymbol{I}_{\mathrm{e}}\ddot{\boldsymbol{\theta}}_1+\boldsymbol{f}_{\mathrm{e}}, \tag{20}$$

$$\boldsymbol{I}_{\mathrm{e}}=\boldsymbol{J}_1^{-\mathrm{T}}\left(\sum_{i=1}^{3}m_{i2}\boldsymbol{U}_i'\boldsymbol{J}_1^{-1}+\boldsymbol{J}_2^{\mathrm{T}}\boldsymbol{I}_2\boldsymbol{J}_2\boldsymbol{J}_1^{-1}+\boldsymbol{I}\boldsymbol{J}_1^{-1}\right)+\boldsymbol{I}_1, \tag{21}$$

$$\boldsymbol{U}_i'=\boldsymbol{U}_i^{\mathrm{T}}\boldsymbol{U}_i,$$

$$\boldsymbol{I}=\begin{bmatrix}m & & \\ & m & \\ & & I\end{bmatrix}.$$

Where f_{e} is a matrix function about $\dot{\theta}_1^2$, $\dot{\theta}_2^2$ and $\dot{\varphi}^2$, which has nothing to do with the inertia.

Since the mass of passive links are the same, assume that $m_{i2}=m_2(i=1,2,3)$. As mentioned early, the moving platform frame $C(O'X'Y'Z')$ is established at the centroid of the moving platform, which is also its geometric center. Thus, the vector sum of $\boldsymbol{c}_i(i=1,2,3)$ is zero. Substituting $\sum_{i=1}^{3}\boldsymbol{c}_i=0$ and $m_{i2}=m_2(i=1,2,3)$ into Eq. (21), a simplified equation can be obtained as

$$\boldsymbol{I}_{\mathrm{e}}=\boldsymbol{J}_1^{-\mathrm{T}}(m_2\boldsymbol{U}'\boldsymbol{J}_1^{-1}+\boldsymbol{J}_2^{\mathrm{T}}\boldsymbol{I}_2\boldsymbol{J}_2\boldsymbol{J}_1^{-1}+\boldsymbol{I}\boldsymbol{J}_1^{-1})+\boldsymbol{I}_1, \tag{22}$$

where

$$\boldsymbol{U}'=\sum_{i=1}^{3}\boldsymbol{U}_i'=\begin{bmatrix}3 & 0 & 0\\ 0 & 3 & 0\\ 0 & 0 & h^2\end{bmatrix}.$$

As shown in Eq. (22), due to the closed-loop structure of the parallel manipulator, the inertia matrix of the parallel manipulator in the actuator space is coupled. Thus, the algebraic expression of the equivalent inertia of the RPKM is unreachable. However, the mean of diagonal elements of the inertia matrix $\boldsymbol{I}_{\mathrm{e}}$ can be used as the numerical result of the equivalent inertia of the RPKM, which can be considered as the average distribution of the sum of the theory inertia. Instead of considering both orientation and position of the moving platform, assume the rotational angle of the moving platform about the Z-axis from the X-axis is permanent zero to simplify the calculation.

4 Numerical Verification of the Equivalent Inertia

Actual values of dynamic parameters of the 3-RRR reconfigurable planar parallel manipulator with aluminum rigid bars, as shown in Table 1, are substituted into the Eq. (22). Then, as shown in Fig. 4, the equivalent inertia is figured out in the required workspace, which is a horizontal circle with the radius of 250 mm [16].

Table 1. Practical values of parameters of the manipulator with aluminium bars

Parameter	Value
Length of drive links l_{i1}/ mm	400
Moment of inertia of drive links I_{i1}/(kg•m^2)	0.012
Mass of passive links m_2/kg	0.197
Length of passive links l_{i2}/mm	400
Moment of inertia of passive links I_{i2}/(kg•m^2)	0.012
Side length of the moving platform h/mm	80
Mass of the moving platform m/kg	0.28
Side length of the base a/mm	900
Moment of inertia of the moving platform I/(kg•m^2)	0.003 04

(i=1,2,3)

Fig. 4 indicates that the range of the equivalent inertia of the reconfigurable parallel manipulator is from 9.87×10^{-2} kg•m^2 to 1.65×10^{-1}kg•m^2, and the equivalent inertia reaches its maximum at the edge of the required workspace. There are three gradient directions, along which the equivalent inertia increase sharply. These three directions are from the center of the workspace to positions of drive rotational joints approximately. Gradient directions show a little counterclockwise rotation, which is determined by the structure of the object.

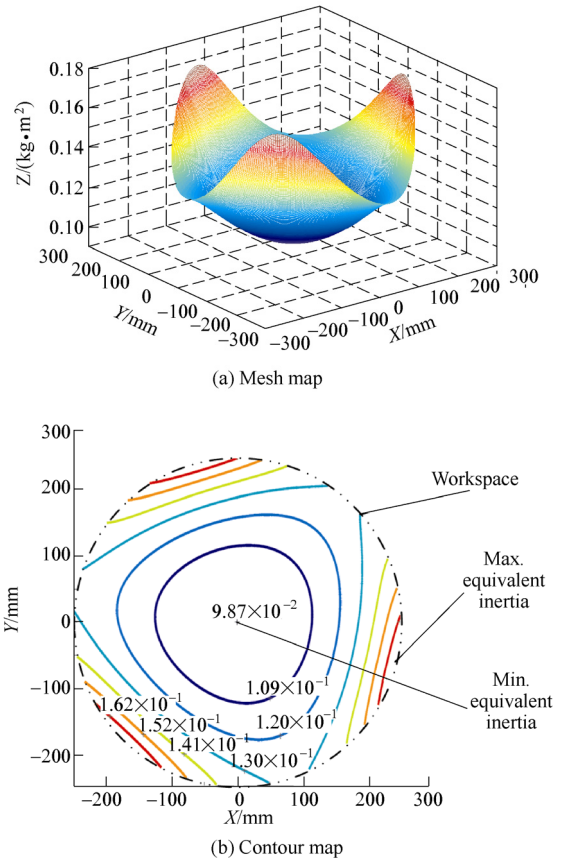

(a) Mesh map

(b) Contour map

Fig. 4. Equivalent inertia of the 3-RRR RPKM

The 3-RRR parallel manipulator can be driven by one drive rotational joint with two others static. At this moment, the 3-RRR parallel manipulator is recursive to a serial multi-bar manipulator. Due to the nature that the moment of inertia is only affected by configuration and posture, the inertia problem of 3-RRR parallel manipulators can be reasonably recursive to that of serial manipulators. Although the motion of the serial multi-bar manipulator is different from that of the 3-RRR parallel manipulator, under the same posture, the inertia of the serial multi-bar manipulator converted to the actuator shaft well equals the inertia of 3-RRR parallel manipulator converted to each actuator in numerical. Thus, it can be used to verify the equivalent inertia deduced by the inertia matrix above.

In order to verify the equivalent inertia of the object shown in Fig. 4, the inertia of the serial multi-bar mechanism converted to the actuator shaft is calculated in the same workspace (a 250-millimeter-radius circular plane), and the orientation angle of the moving platform is kept zero, too. Eqs. (3) and (4) are used to obtain the posture of the serial multi-bar manipulator in every position of the required workspace.

Due to the circular symmetrical configuration of the 3-RRR RPKM, assume that drive rotational joints A_1 and A_2 are static. Then, the serial multi-bar manipulator, which consists of B_1C_1, B_2C_2, the moving platform, B_1C_1 and A_1B_1, is actuated by the drive joint A_3. As all notations have been described in section 3, they are not repeated here.

Forward vector loop equations can be written in the global frame as follows:

$$\boldsymbol{r}+\boldsymbol{Rc}_1=l_{12}\boldsymbol{s}_{12}+\boldsymbol{b}_1, \tag{23}$$

$$\boldsymbol{r}+\boldsymbol{Rc}_2=l_{22}\boldsymbol{s}_{22}+\boldsymbol{b}_2, \tag{24}$$

$$\boldsymbol{r}+\boldsymbol{Rc}_3=l_{31}\boldsymbol{s}_{31}+l_{32}\boldsymbol{s}_{32}, \tag{25}$$

where $\boldsymbol{b}_1=\boldsymbol{r}_{A1}+l_{11}\boldsymbol{s}_{11}$, $\boldsymbol{b}_2=\boldsymbol{r}_{A2}+l_{21}\boldsymbol{s}_{21}$.

Forward velocity mapping functions can be found by taking the derivative of Eqs. (23), (24), and (25) with respect to time:

$$\dot{\boldsymbol{r}}+\boldsymbol{W}\times\boldsymbol{Rc}_1=l_{12}\boldsymbol{W}_{12}\times\boldsymbol{s}_{12}, \tag{26}$$

$$\dot{\boldsymbol{r}}+\boldsymbol{W}\times\boldsymbol{Rc}_2=l_{22}\boldsymbol{W}_{22}\times\boldsymbol{s}_{22}, \tag{27}$$

$$\dot{\boldsymbol{r}}+\boldsymbol{W}\times\boldsymbol{Rc}_3=l_{31}\boldsymbol{W}_{31}\times\boldsymbol{s}_{31}+l_{32}\boldsymbol{W}_{32}\times\boldsymbol{s}_{32}. \tag{28}$$

Taking the dot product of Eqs. (26), (27), and (28) correspondingly with $\boldsymbol{s}_{12}$, $\boldsymbol{s}_{22}$ and $\boldsymbol{s}_{32}$, the velocity of the moving platform can be described by the input angular velocity of the drive joint A_3 as

$$\boldsymbol{A}\dot{\boldsymbol{p}}=\dot{\theta}_{31}\boldsymbol{n}, \tag{29}$$

where

$$\boldsymbol{A}=\begin{bmatrix}\cos\theta_{12} & \sin\theta_{12} & x_{Rc_1}\sin\theta_{12}-y_{Rc_1}\cos\theta_{12}\\ \cos\theta_{22} & \sin\theta_{22} & x_{Rc_2}\sin\theta_{22}-y_{Rc_2}\cos\theta_{22}\\ \cos\theta_{32} & \sin\theta_{32} & x_{Rc_3}\sin\theta_{32}-y_{Rc_3}\cos\theta_{32}\end{bmatrix}.$$

By using of Eqs. (1) to (4), unit vectors along passive and drive links can be obtained. Simultaneously, taking $\dot{\theta}_{31}$ and $\dot{\boldsymbol{p}}$ into Eqs. (26), (27), and (28), $\dot{\theta}_{12}$, $\dot{\theta}_{22}$ and $\dot{\theta}_{32}$ can be deduced. Further, according to the equivalent inertia principle of serial mechanisms, the inertia of the serial manipulator converted to the actuator shaft is obtained as

$$I_{\text{load}}=I_{31}+m_2l_{31}^2+I_{32}(\dot{\theta}_{32}/\dot{\theta}_{31})^2+I_{12}(\dot{\theta}_{12}/\dot{\theta}_{31})^2+I_{22}(\dot{\theta}_{22}/\dot{\theta}_{31})^2+m(\dot{x}/\dot{\theta}_{31})^2+m(\dot{y}/\dot{\theta}_{31})^2+I(\dot{\varphi}/\dot{\theta}_{31})^2.$$

Taking practical values of parameters, which are shown

in Table 1, into the above equation, the distribution map of the inertia of the serial multi-bar manipulator is obtained, as shown in Fig. 5.

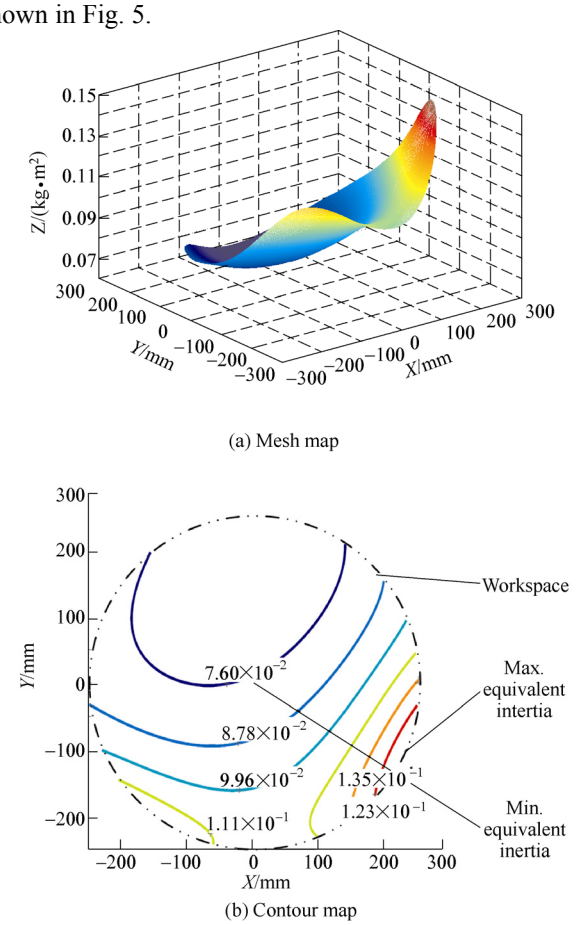

Fig. 5. Inertia of the serial manipulator converted to the actuator

Examination of Fig. 5 indicates following conclusions:

(1) The range of the inertia of the serial manipulator converted to the actuator is from 7.60×10^{-2} kg•m^2 to 1.35×10^{-1} kg•m^2, which verifies the equivalent inertia of the RPKM obtained in section 3 to some extent in value.

(2) The distribution of the equivalent inertia of the RPKM, as shown in Fig. 4, can be regard as the stacking of inertias of serial manipulators independently actuated by A_1, A_2 and A_3 in turn, which verifies the equivalent inertia in distribution.

In all, the equivalent inertia of the RPKM and the recursive method are mutually verified, can well reflect the distribution and value of the inertial load of the parallel manipulator converted to each actuator shaft. The result obtained through the recursive serial method is incomplete, and cannot replace the equivalent inertia deduced from inertial matrix. It is because the parallel manipulator is inherently coupled, which is missing in the recursive way. Besides, the equivalent inertia can be obtained conveniently from inverse dynamic formulations, which are already obtained in the calculation of required rated torque of actuators. Thus, the analysis and application, in the following sections, are all based on the equivalent inertia.

5 Analysis

In this section, analysis on the equivalent inertia of the 3-RRR reconfigurable planner parallel manipulator is carried out.

Examining Fig. 4, some useful conclusions can be drawn on the distribution of the equivalent inertia of the 3-RRR RPKM in the workspace.

(1) The distribution of the equivalent inertia is circular symmetrical, which is determined by the configuration feature of the 3-RRR parallel manipulator.

(2) The variation of the equivalent inertia reflects changes of Jacobian matrixes. And, clues can be found in Eq. (22).

(3) In trajectory planning, since the equivalent inertia increases gradually from the centre to the edge in the required workspace, the region around centre should be fully utilized.

(4) Although the required workspace of the 3-RRR RPKM is circular, the suggested workspace is triangular.

Beneath, let's take a closer look at contributions of each part of the 3-RRR RPKM to the equivalent inertia.

According to differences of the physical meaning, Eq. (22) can be written as

$$\boldsymbol{I}_{\mathrm{e}} = \boldsymbol{I}_1 + \boldsymbol{I}_2' + \boldsymbol{I}_2'' + \boldsymbol{I}', \tag{30}$$

where

$$\boldsymbol{I}_2' = \boldsymbol{J}_1^{-\mathrm{T}} \boldsymbol{J}_2^{\mathrm{T}} \boldsymbol{I}_2 \boldsymbol{J}_2 \boldsymbol{J}_1^{-1}, \tag{31}$$

$$\boldsymbol{I}_2'' = m_2 \boldsymbol{J}_1^{-\mathrm{T}} \boldsymbol{U}' \boldsymbol{J}_1^{-1}, \tag{32}$$

$$\boldsymbol{I}' = \boldsymbol{J}_1^{-\mathrm{T}} \boldsymbol{I} \boldsymbol{J}_1^{-1}. \tag{33}$$

The motion of a rigid body can be divided into the rotation around some point and the movement with the point. $\boldsymbol{I}_2'$, which is converted from the inertia matrix of passive link $\boldsymbol{I}_2$, indicates the rotation of passive links about pivotal points C_i. However, $\boldsymbol{I}_2''$, which is converted from the mass of passive links and the dimension matrix of the manipulator ($\boldsymbol{U}'$), indicates the movement of passive links with pivotal points C_i. $\boldsymbol{r}$, which is converted from the mass and inertia matrix of the moving platform $\boldsymbol{I}$, indicates the motion of the moving platform. $\boldsymbol{I}_1$ is the inertia matrix of drive links, and can be converted to the actuator shaft directly without any change.

By calculation separately, distributions of the equivalent inertia contributed by these three parts of the RPKM are obtained, as shown in Figs. 6, 7, and 8.

Although drive and passive links possess the same mass and inertia, the contribution of passive links $\boldsymbol{I}_2' + \boldsymbol{I}_2''$ to the equivalent inertia is much larger than that of drive links. As shown in Fig. 9, the contribution percentage of passive links is as high as 66%. It's because that the 3-RRR planar parallel manipulator under this configuration can get a high terminal velocity while drive rotational joints rotate at relative low speeds. In other words, it is the type of manipulator with large speed amplification ratio, like Delta

and Diamond robots. The inertia and mass of passive links, therefore, should not be neglected when simplifying the inverse dynamics, especially in the process of the inertia match of the parallel manipulator with large speed amplification ratio.

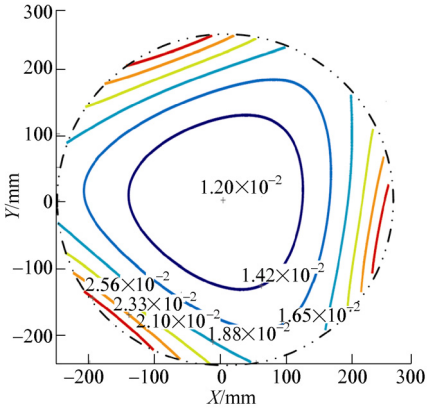

Fig. 6. Contribution of I_2'

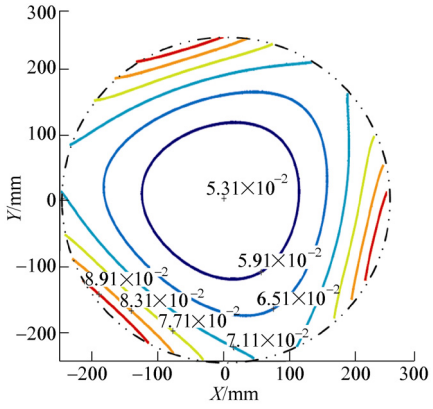

Fig. 7. Contribution of I_2''

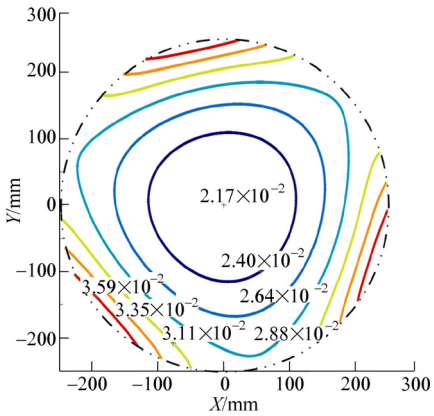

Fig. 8. Contribution of I'

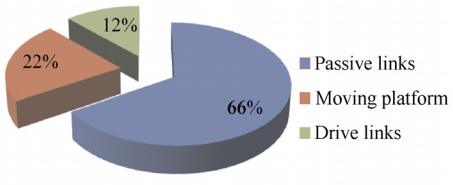

Fig. 9. Contribution percentages of each part

6 Application

In this section, the equivalent inertia of the RPKM is used to accomplish the inertia match of the 3-RRR reconfigurable planar parallel manipulator under three different stiffness configurations. The manipulator is equipped with light flexible bars, rigid aluminum bars and rigid steel bars in turn. The servo motor is selected first according to the rated torque and power, and its moment of inertia is 2.6×10^{-3} kg•m^2. Considering that the equivalent inertia should be less than three times of the motor inertia to obtain good dynamic performance (generally referring to acceleration and deceleration capacities) while the recommended ratio is 2.5[17], the inertia match is accomplished by matching appropriate reducers.

Table 2. Inertia match result

Bar suite	Reduction ratio	Maximal equivalent inertia I_{emax}/(kg•m^2)	Performance without reducers	Performance with reducers
Light flexible bars	1:3	6.18×10^{-2}	Acceptable	Good
Alumi-nium bars	1:5	1.65×10^{-1}	Poor	Good
Steel bars	1:8	4.28×10^{-1}	Out of control	Good

As shown in Table 2, without reducers, when equipped with light flexible bars, the dynamic performance of the manipulator is barely acceptable. But when equipped with steel bars, the manipulator is uncontrollable and vibrates fiercely. And, when equipped with aluminum bars, the manipulator is under control, but the dynamic performance is poor. However, the manipulator, when matched with corresponding reducers, can work well in different configurations. Finally, the inertia match of the 3-RRR reconfigurable planar parallel manipulator is accomplished, which also proofs the necessity of the inertia match and the practicality of the equivalent inertia.

7 Conclusions

(1) In order to guarantee excellent kinematics and dynamics performance, when choosing motor, the inertia match of the parallel manipulator should be fulfilled on the basis of matches of required maximum speed, maximum torque, rated power, and so on.

(2) The inertia matrix of the 3-RRR reconfigurable planar parallel manipulator can be obtained on the basis of the inverse dynamic formulation derived by adopting the principle of virtual work.

(3) On the basis of inverse dynamics, the equivalent inertia of the parallel manipulator is a convenient and practical way to accomplish the inertia match.

(4) In the process of calculating the equivalent inertia of the 3-RRR parallel manipulator, the inertia and mass of passive links should not be neglected when simplifying the inverse dynamics, especially for the configurations with the large speed amplification ratio feature.

(5) According to the distribution of the equivalent inertia of the 3-RRR RPKM, the suggested workspace is triangular.

(6) Since the equivalent inertia increases gradually with the platform moving from the geometric centre to the edge in the required workspace, the 3-RRR RPKM can get better dynamic performance when the platform moves around the workspace centre.

References

[1] SHI Junshan, TANG Xiaoqiang, LIN Chunshen, et al. Comparison study of two tricept units for reconfigurable parallel kinematic machines[J]. *High Technology Letters*, 2005, 11(12): 392–396.

[2] YANG Jianxin, YU Dingwen, WANG Liping. Progress in the research of parallel machine tool[J]. *Mechanical Design and Manufacture Engineering*, 2002, 31(03): 10–14. (in Chinese)

[3] GAO Meng, LI Tiemin, TANG Xiaoqiang. The Calibration Study on Low Mobility parallel machines[J]. *Chinese Journal of Mechanical Engineering*, 2003, 39(9): 118–122. (in Chinese)

[4] FISHER R, PODHORODESKI R P, NOKLEBY S B. Design of a reconfigurable planar parallel manipulator[J]. *Journal of Robotic Systems*, 2004, 21(12): 665–675.

[5] DASGUPTA B, MRUTHYUNJAYA T S. Closed-form dynamic equations of the general Stewart platform through the Newton-Euler approach [J]. *Mechanism* and *Machine Theory*, 1998, 33(7): 993–1012.

[6] DASGUPTA B, CHOUDHURY P. A general strategy based on the Newton-Euler approach for the dynamic formulation of parallel manipulators[J]. *Mechanism and Machine Theory*, 1999, 34(6): 801–824.

[7] DASGUPTA B, MRUTHYUNJAYA T S. A Newton-Euler formulation for the inverse dynamics of the Stewart platform manipulator [J]. *Mechanism* and *Machine Theory*, 1998, 33(8): 1 135– 1 152.

[8] LI Yangmin, XU Qingsong. Kinematics and inverse dynamics analysis for a general 3-PRS spatial parallel mechanism[J]. *Robotic*, 2005, 23(2): 219–229.

[9] LEBRET G, LIU K, LEWIS F L. Dynamic analysis and control of a Stewart platform manipulator[J]. *Journal of Robotic Systems*, 1993, 10(5): 629–655.

[10] SOKOLOV A, XIROUCHAKIS P. Dynamics analysis of a 3-DOF parallel manipulator with R-P-S joint structure[J]. *Mechanism and Machine Theory*, 2007, 42(5): 541–557.

[11] TSAI L W. Solving the inverse dynamics of a Stewart-Gough manipulator by the principle of virtual work[J]. *Journal of Mechanical Design*, 2000, 122(1): 3–9.

[12] ZHANG C D, SONG M S. An efficient method for inverse dynamics of manipulators based on the virtual work principle[J]. *Journal of Robotic Systems*, 1993, 10(5): 605–627.

[13] HUANG Tian, MEI JiangPing, LI Zhanxian, et al. A method for estimating servomotor parameters of a parallel robot for rapid pick-and-place operations[J]. *Journal of Mechanical Design*, 2005, 127(4): 596–601.

[14] Zhiming Ji, Philip Song. Design of a reconfigurable platform manipulator [J]. *Journal of Robotic Systems*, 1998, 15(6): 341–346.

[15] GOSSELIN, C. *Kinematic analysis, optimization and programming of parallel robotic manipulators* [D]. Montreal: McGill University, 1988.

[16] YAO Rui, TANG Xiaoqiang, HUANG Peng, et al. Dimensional design of flexible 3-RRR planar parallel manipulator with high acceleration [J]. *Journal of Tsinghua University (Scinence and Technology)*, 2008, 48(2): 184–188. (in Chinese)

[17] Fanuc AC Servo Motor αi/αis Descriptions Manual B-65262EN/03 [EB/OL].North America: GE Fanuc Automation, 2003[2009-8-9]. http://fanuc.pennineuk.com/library/pdf/AIMANUAL.pdf.

Biographical notes

SHAO Zhufeng, born in 1983, is currently a PhD candidate in Department of Precision Instruments and Mechanology, Tsinghua University, China. He received his bachelor degree from Shandong University, China, in 2006. His research interests include parallel robotics and its dynamic control.
Tel: +86-10-62792678;
E-mail: shaozf06@mails.tsinghua.edu.cn

TANG Xiaoqiang, born in 1973, is currently an associate professor in Department of Precision Instruments and Mechanology, Tsinghua University, China. He received his PhD degree from Tsinghua University, China, in 2001. His research interests include reconfigurable manufacture system, parallel manipulator.
E-mail: tang-xq@mail.tsinghua.edu.cn

CHEN Xu, born in 1974, is currently a post doctor in Department of Precision Instruments and Mechanology, Tsinghua University, China. He received his PhD degree from Jilin University, China, in 2006. His research interests include parallel manipulator, dynamic control。
E-mail: chxu@mail.tsinghua.edu.cn

WANG Liping, born in 1967, is currently a professor in Department of Precision Instruments and Mechanology, Tsinghua University, China. His research interests include parallel machine tools and its dynamic control.
E-mail: Lpwang@mail.tsinghua.edu.